Journal of Nuclear Materials 486 (2017) 216–221

Contents lists available at ScienceDirect

Journal of Nuclear Materials

journal homepage: www.elsevier.com/locate/jnucmat

Raman study on structure of $U_{1-y}Gd_yO_{2-x}$ (y=0.005, 0.01, 0.03, 0.05 and 0.1) solid solutions

Jeongmook Lee [a], Jandee Kim [a], Young-Sang Youn [a], Nazhen Liu [b], Jong-Goo Kim [a], Yeong-Keong Ha [a], David W. Shoesmith [b], Jong-Yun Kim [a, c, *]

[a] Nuclear Chemistry Research Division, Korea Atomic Energy Research Institute, 111 Daedeok-daero 989 Beon-gil, Yuseong-gu, Daejeon, 34057, Republic of Korea
[b] Department of Chemistry, Western University, London, Ontario N6A 5B7, Canada
[c] Department of Radiochemistry & Nuclear Nonproliferation, University of Science & Technology, Gajeong-ro 217, Yuseong-gu, Daejeon, 34113, Republic of Korea

HIGHLIGHTS

- Investigation of structural character of $U_{1-y}Gd_yO_{2-x}$ solid solutions.
- Defect structures in $U_{1-y}Gd_yO_{2-x}$ solid solutions were evaluated by Raman spectroscopy.
- Oxygen deficiency due to Gd content causes Raman band related to oxygen vacancy.

ARTICLE INFO

Article history:
Received 27 October 2016
Received in revised form
8 December 2016
Accepted 3 January 2017
Available online 5 January 2017

Keywords:
Gadolinium doping
Uranium dioxide
Solid solution
X-ray diffraction
Raman spectroscopy
Defect structure
Oxygen vacancy

ABSTRACT

The $U_{1-y}Gd_yO_{2-x}$ solid solutions with y = 0.005, 0.01, 0.03, 0.05 and 0.1 were characterized by Raman spectroscopy to investigate the defect structure induced by oxygen vacancies. The oxygen deficiencies of solid solutions were estimated by the relation between the doping level and a lattice parameter calculated from X-ray diffraction patterns. Raman mode shifts to higher wavenumber with increasing doping level showed that crystal lattice disorder due to oxygen vacancies. The frequency shifts and relative ratio of Raman modes were enabled to be the indicator for composition, defect and oxygen vacancy of $U_{1-y}Gd_yO_{2-x}$ solid solutions.

1. Introduction

In reactor irradiation of UO_2 nuclear fuel leads to the formation of a wide range of fission products, transuranium elements and activation products [1–3]. Among them rare earth (RE) elements form $U_{1-y}RE_yO_2$ solid solutions with UO_2 [4]. When irradiated under reducing circumstances, to a high burnup in the range of 70–80 GWd/tU, the UO_2 fuel becomes doped with fission products (FPs), especially rare earths, and can be considered as a slightly sub-stoichiometric ($U_{1-y}FP_yO_{2-x}$) or stoichiometric compound [5]. A knowledge of the structural character of RE-doped $UO_{2\pm x}$ is very important not only to understand the characteristics of spent nuclear fuel but also to describe the thermodynamic properties and the phase relations in U-RE-O systems [6–9]. Among the many RE elements, Gd is one of the major fission products formed in solid solution with UO_2 and has often been selected as a dopant in simulated spent nuclear fuels [10–12]. It is also used as a burnable absorber for the UO_2-Gd_2O_3 fuels developed to extend the length of the fuel cycle for PWRs [13]. Thus, Gd-doped UO_2 has been extensively researched using several experimental techniques, generally in tandem with X-ray diffraction (XRD) [14–20], to understand its physical and chemical properties.

* Corresponding author. Nuclear Chemistry Research Division, Korea Atomic Energy Research Institute, 111 Daedeok-daero 989 Beon-gil, Yuseong-gu, Daejeon, 34057, Republic of Korea.
E-mail address: kjy@kaeri.re.kr (J.-Y. Kim).

http://dx.doi.org/10.1016/j.jnucmat.2017.01.004
0022-3115/

Recently, Raman spectroscopy has been widely applied to characterize nuclear fuel materials, because it is a convenient, sensitive and nondestructive method [21]. For example, the effect of oxygen stoichiometry on the defect structure of UO_2 [22,23], the oxygen sublattice structure in thorium dioxide-uranium dioxide fuel materials [24] and the influence of trivalent-dopants on the structural properties of UO_2 [25] have been investigated in detail using Raman spectroscopy. The role of oxygen vacancies on the kinetics of oxidation of fuel have also been demonstrated in Raman studies of Gd-, Dy-doped UO_2 [25], $U_{1-y}Nd_yO_{2-x}$ [26], $U_{1-y}La_yO_{2-y/2}$ [27], and $U_{1-y}Am_yO_{2-x}$ [28] samples. The oxygen vacancy can be created to maintain electroneutrality in RE(III)-doped UO_2 when RE(III) is substituted for U(IV) in solid solutions.

In this study we have characterized the effect of Gd-doping on the structure ($U_{1-y}Gd_yO_{2-x}$) using XRD and Raman spectroscopy to identify the possible defect structures in nuclear fuel materials. Defect structures of $U_{1-y}Gd_yO_{2-x}$ solid solutions with various Gd doping levels were analyzed, and the results compared with published literature.

2. Experimental

$U_{1-y}Gd_yO_{2-x}$ solid solution pellets with various composition (y = 0.005, 0.01, 0.03, 0.05 and 0.1) were synthesized by a conventional solid-state reaction with powder mixing. Appropriate amounts of UO_2 and Gd_2O_3 (Aldrich, >99.99%) powders to achieve the intended composition were blended thoroughly in an agar mortar. The mixtures were then pressed into a disk-shaped pellet and sintered in an alumina tube furnace (Ajeon Heating Industrial, Korea) at 1700 °C for 18 h under a reducing atmosphere with flowing H_2 to produce $U^{4+}{}_{1-y}Gd^{3+}{}_yO^{2-}{}_{2-y/2}$ type solid solutions [8,15]. The sintered pellets were cooled to room temperature in flowing H_2 after annealing in the same atmosphere at 1200 °C for 12 h. An undoped UO_2 pellet was also prepared using the same procedure. After sintering, the pellets were stored in a vacuum chamber to prevent surface oxidation before measuring XRD and Raman spectra.

The X-ray diffraction (XRD) patterns of the $U_{1-y}Gd_yO_{2-x}$ solid solution pellets were performed using a Bruker AXS D8 Advance X-ray Diffractometer using CuKα radiation at room temperature. XRD data was collected in the range from 20° to 120° using a 0.02° step size. These analyses required the exposure of the specimens to air for a total time of only 500 s. Data was collected from several locations to confirm the solid structure was homogeneous. The lattice parameters were calculated by a refinement process using the TOPAS program (Bruker Analytical X-Ray Systems) with the $Fm\bar{3}\,m$ space group.

The Raman spectra were measured with an ANDOR Shamrock SR500i spectrometer, with active vibrations excited using a He-Ne laser with a wavelength of 632.8 nm. The laser with *c.a.* 5 mW power was focused onto the pellets using an Olympus microscope with a 50-fold magnification lens. This laser power was confirmed as low enough to prevent surface oxidation of the pellets due to local heating by the laser beam [29]. Raman spectra were acquired over the wavenumber range 400–1200 cm^{-1} at room temperature with an exposure time to air of 300 s. Raman spectra were measured at different locations on the surface of a pellet to confirm the homogeneity of the pellet and the reproducibility of the spectra.

3. Results and discussion

XRD patterns for UO_2 and a number of $U_{1-y}Gd_yO_{2-x}$ pellets with different Gd contents are shown in Fig. 1(a). All the specimens exhibit the fluorite structure and no XRD peaks for monoclinic

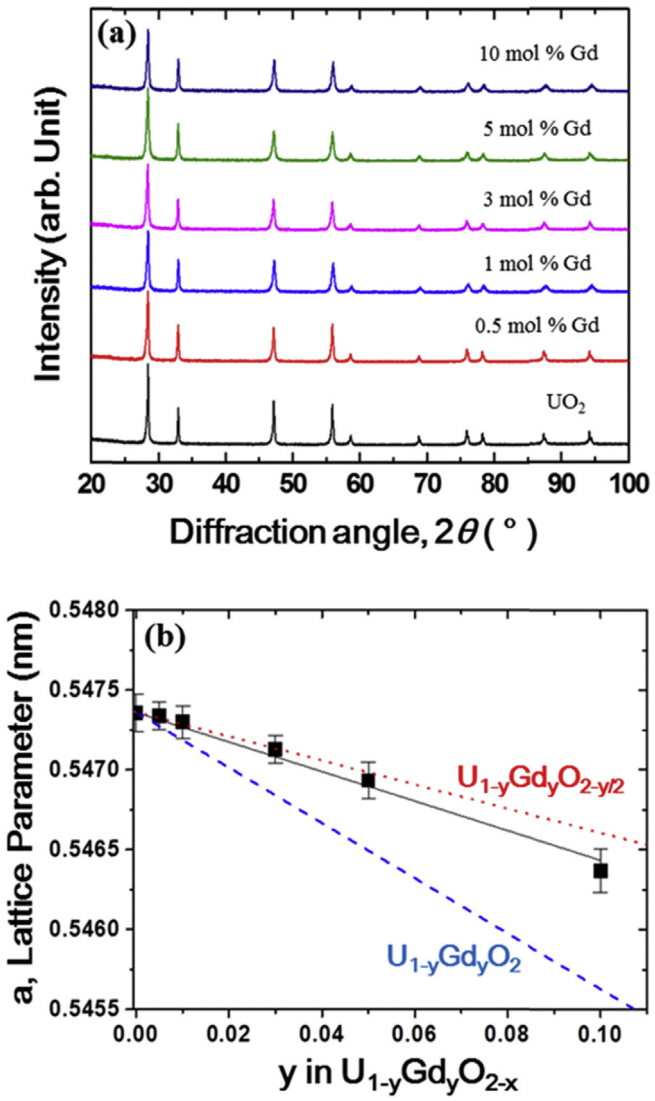

Fig. 1. (a) XRD patterns of UO_2 and $U_{1-y}Gd_yO_{2-x}$ solid solutions with y = 0.005, 0.01, 0.03, 0.05 and 0.1. (b) The lattice parameters obtained from XRD patterns of UO_2 and $U_{1-y}Gd_yO_{2-x}$ solid solutions with increasing Gd concentration. The red dotted and blue dashed lines show the linear relationships obtained for $U_{1-y}Gd_yO_{2-y/2}$ and $U_{1-y}Gd_yO_2$ solid solutions, respectively, as the Gd content changes [15]. (For interpretation of the references to colour in this figure legend, the reader is referred to the web version of this article.)

Gd_2O_3 and undoped UO_2 were observed in the range $25° < 2\theta < 35°$ in contrast to patterns recorded on Gd_2O_3-dispersed UO_2 in which Gd_2O_3 particles are dispersed within the UO_2 matrix [30]. The lattice parameters of the pellets obtained from these patterns are plotted as a function of Gd content in Fig. 1(b). In contrast to the minor change in lattice parameter observed with increasing Gd content for the Gd_2O_3-dispersed UO_2 [30], the lattice parameter for the series $U_{1-y}Gd_yO_{2-x}$ solid solutions decreases linearly with the increase in Gd content. Our linear relationship for $U_{1-y}Gd_yO_{2-x}$ solid solutions is less steep than that observed for $U_{1-y}Gd_yO_2$-type solid solutions, but well-matched with that of $U_{1-y}Gd_yO_{2-x}(x \approx y/2)$-type solid solutions [15]. Lanthanide-doped UO_2 ($U_{1-y}La_yO_{2-y/2}$) solid solutions also exhibited a linear relationship between the lattice parameter and the lanthanum content [27]. This analysis shows our pellets are sub-stoichiometric $U_{1-y}Gd_yO_{2-x}(x \approx y/2)$ solid solutions in the given range y = 0.005–0.05.

Although it is quite difficult to measure the accurate oxygen-to-metal (O/M) ratio for rare earth-doped uranium dioxides, Ohmichi

et al. [15] deduced the relationship between the lattice parameter (a) and the value of x in $U_{1-y}Gd_yO_{2-x}$ type solid solutions with constant y to be da/dx = 0.024 ± 0.006 nm. This equation was derived using O/M ratio data by chemical analysis and the lattice parameter values by XRD analysis. Using this relationship, the O/M ratios of the sintered $U_{1-y}Gd_yO_{2-x}$ pellets is estimated and plotted as a function of Gd content in Fig. 2. Those values closely match the results obtained for $U_{1-y}Gd_yO_{2-x}$(x ≈ y/2)-type solid solutions in the published study [15]. The $U_{0.9}Gd_{0.1}O_{2-x}$ pellet, however, has a higher O/M ratio than expected due possibly to oxidation during handling or a lack of reducing power during sintering.

Fig. 3 shows Raman spectra recorded on the UO_2 and $U_{1-y}Gd_yO_{2-x}$ (y = 0.005, 0.01, 0.03, 0.05 and 0.1) specimens. The spectra are the averaged spectra from 10 different locations on the pellets. Some inhomogeneity was observed for spectra from different locations on the $U_{1-y}Gd_yO_{2-x}$ pellets due to the dry mixing process that leads to some inhomogeneous distribution of the cations [16]. However, as will be shown below, these differences do not disguise the ability to observe the changes in the spectra as Gd content varies.

Raman spectra recorded on undoped UO_2 exhibit the spectral features expected for an undistorted fluorite structure at 445 cm^{-1} and at 1150 cm^{-1}. The peak at 445 cm^{-1} can be attributed to the triply degenerate Raman active T_{2g} mode for the U-O symmetric stretching mode in the fluorite structure of UO_2 [31–33]. The broad peak at 1150 cm^{-1} has been assigned to an overtone (2L-O) of the first order longitudinal optical (L-O) phonon regarded as a fingerprint for a quasi-perfect fluorite structure [22,34]. The very shallow feature located at 575 cm^{-1} can be ascribed to a first order L-O phonon at the center of the Brillouin zone [35].

Raman spectra recorded on the $U_{1-y}Gd_yO_{2-x}$ pellets showed the development of a broad band in the spectral region 500 to 650 cm^{-1}, and a dramatic decrease in intensity of peaks at 445 cm^{-1} and at 1150 cm^{-1} as the Gd doping level increased. These spectral changes are similar to those observed for hyper-stoichiometric UO_{2+x}, due to the defects introduced by hyper–stoichiometric oxygen [23], and for La-doped UO_2 due to the distortion of lattice structure induced by doping [27]. The decreasing T_{2g} and 2L-O modes with increasing Gd contents indicate distortion of the fluorite UO_2 lattice structure due to the Gd^{3+} doping. The Raman spectra were analyzed by deconvoluting the broad band in the spectral region from 500 to 650 cm^{-1} into three bands (Fig. 4). The

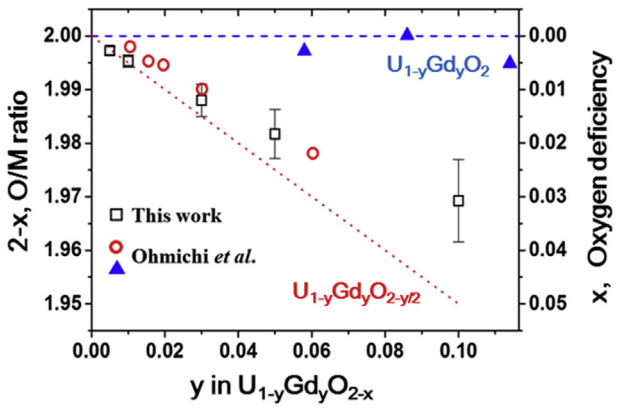

Fig. 2. The black squares show the O/M ratio (2−x) and oxygen deficiency (x) for $U_{1-y}Gd_yO_{2-x}$ solid solutions calculated using da/dx = 0.024 ± 0.006 nm from Ref. [15]. The red circles and blue triangles show the experimental values for $U_{1-y}Gd_yO_{2-x}$(x ≈ y/2)-type and $U_{1-y}Gd_yO_2$ solid solutions, respectively (from Ref. [15]). The red dotted and blue dashed lines show the ideal O/M ratios for perfect $U_{1-y}Gd_yO_{2-y/2}$ and $U_{1-y}Gd_yO_2$ solid solutions as a function of Gd content, respectively. (For interpretation of the references to colour in this figure legend, the reader is referred to the web version of this article.)

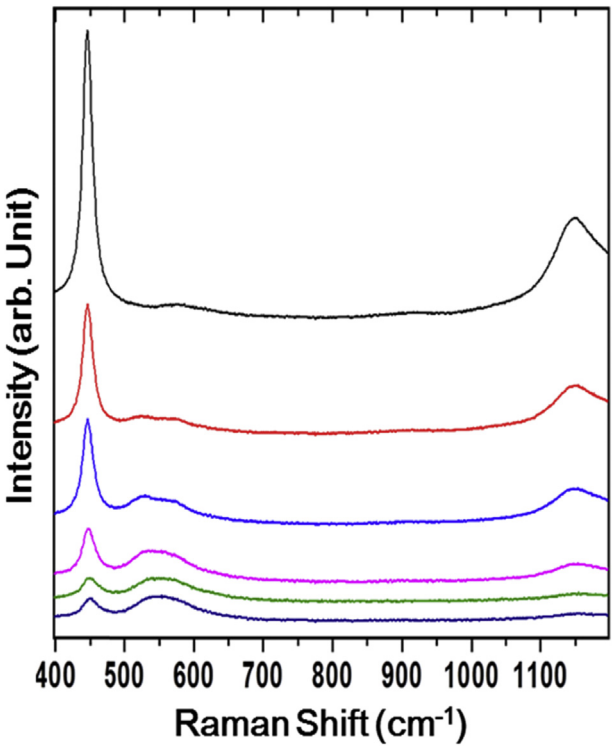

Fig. 3. Raman spectra of UO_2 and $U_{1-y}Gd_yO_{2-x}$ solid solutions with y = 0.005, 0.01, 0.03, 0.05 and 0.1 from top to bottom.

peaks at ~445, ~530, ~575 and ~630 cm^{-1} are denoted as T_{2g}, α, β and γ, respectively. The frequency shifts for each peak varied slightly with increasing Gd content, as observed previously for $(U,Am)O_{2-\delta}$ samples [28]. The averaged frequencies used to fit the broad bands in the 500 to 650 cm^{-1} region for all measured Raman spectra are plotted as a function of Gd content for the T_{2g}, α and β peaks in Fig. 5.

The peak T_{2g} at ~445 cm^{-1} in Raman spectra of $U_{1-y}Gd_yO_{2-x}$ pellets shows a shift to higher wavenumbers is accompanied by a marked decrease in intensity with increasing Gd doping level. Raman spectra recorded on RE(III)-doped UO_2 [25] and CeO_2 [36] showed similar features due to the structural distortions of the fluorite lattice caused by the RE(III) doping. McBride et al. [36] suggested this frequency shift for the T_{2g} mode $Ce_{1-y}RE_yO_{2-x}$ samples is caused by contraction of the lattice, and can be attributed to the creation of oxygen vacancies to offset the charge imbalance due to RE(III) doping. In our case, the decrease in lattice parameter (a) with increasing Gd doping indicates a contraction of the UO_2 lattice and an increase in the oxygen vacancy concentration required to balance the charge of the $U_{1-y}Gd_yO_{2-x}$ solid solution. These changes in lattice structure of the UO_2 result in the positive frequency shift of the T_{2g} mode with increasing Gd content. This frequency shift may be useful in quantitative analysis of $U_{1-y}Gd_yO_{2-x}$ solid solutions. The linear dependence of the T_{2g} mode in $U_{1-y}Gd_yO_{2-x}$ solid solutions on Gd content (64 ± 7 cm^{-1} per y) could be used to estimate the Gd content of doped matrices of uncertain composition.

The peak α at ~530 cm^{-1} in the broad band in the region 500-650 cm^{-1} is not observed for pure UO_2 and is attributed to the presence of the oxygen vacancies associated with Gd^{3+}. Razdan and Shoesmith [25] also observed this peak and attributed it to the creation of oxygen vacancies in Gd-doped and Dy-doped UO_2, and Talip et al. [27] also demonstrated the existence of oxygen vacancies in UO_2 with 6, 11, 22 mol% La by Raman spectroscopy. These

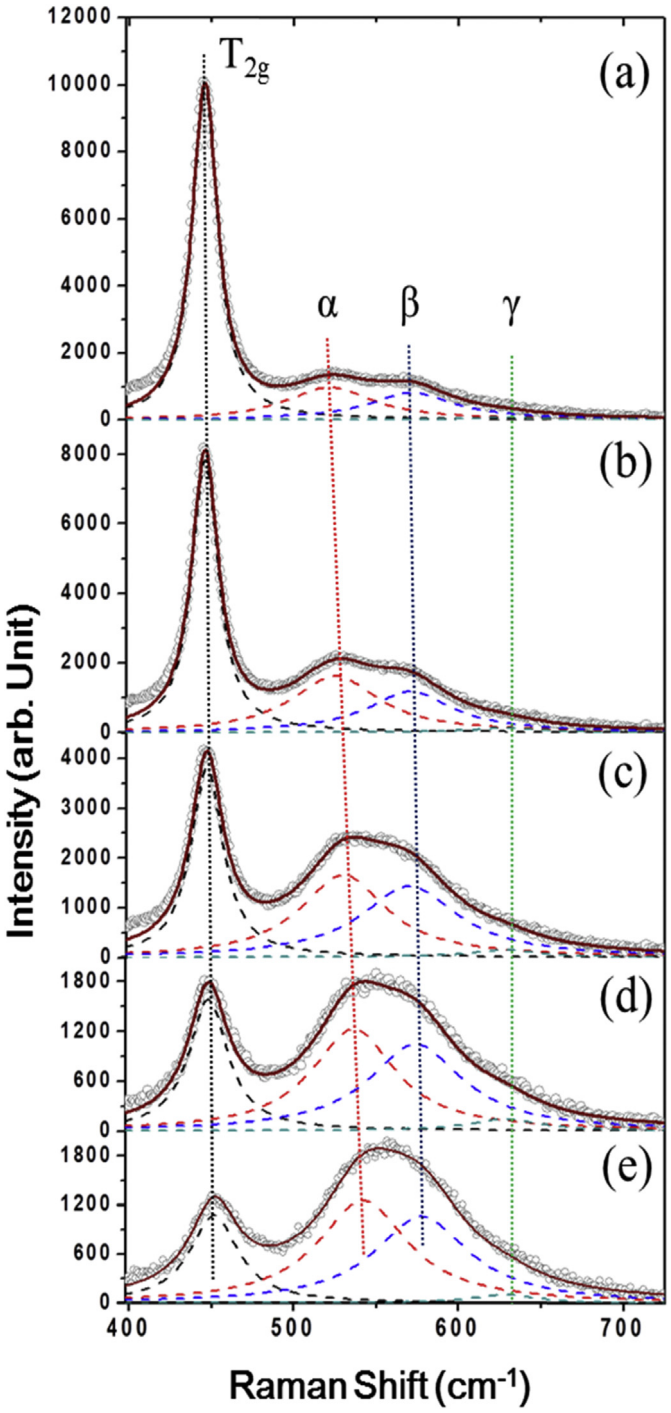

Fig. 4. Deconvoluted Raman spectra of (a) $U_{0.995}Gd_{0.005}O_{2-x}$, (b) $U_{0.99}Gd_{0.01}O_{2-x}$, (c) $U_{0.97}Gd_{0.03}O_{2-x}$, (d) $U_{0.95}Gd_{0.05}O_{2-x}$ and (e) $U_{0.9}Gd_{0.1}O_{2-x}$ solid solutions with dashed Lorentzian peaks at ~445, 530, 575 and 630 cm^{-1}. Gray dots and brown line represent the experimental data and fitted line, respectively. (For interpretation of the references to colour in this figure legend, the reader is referred to the web version of this article.)

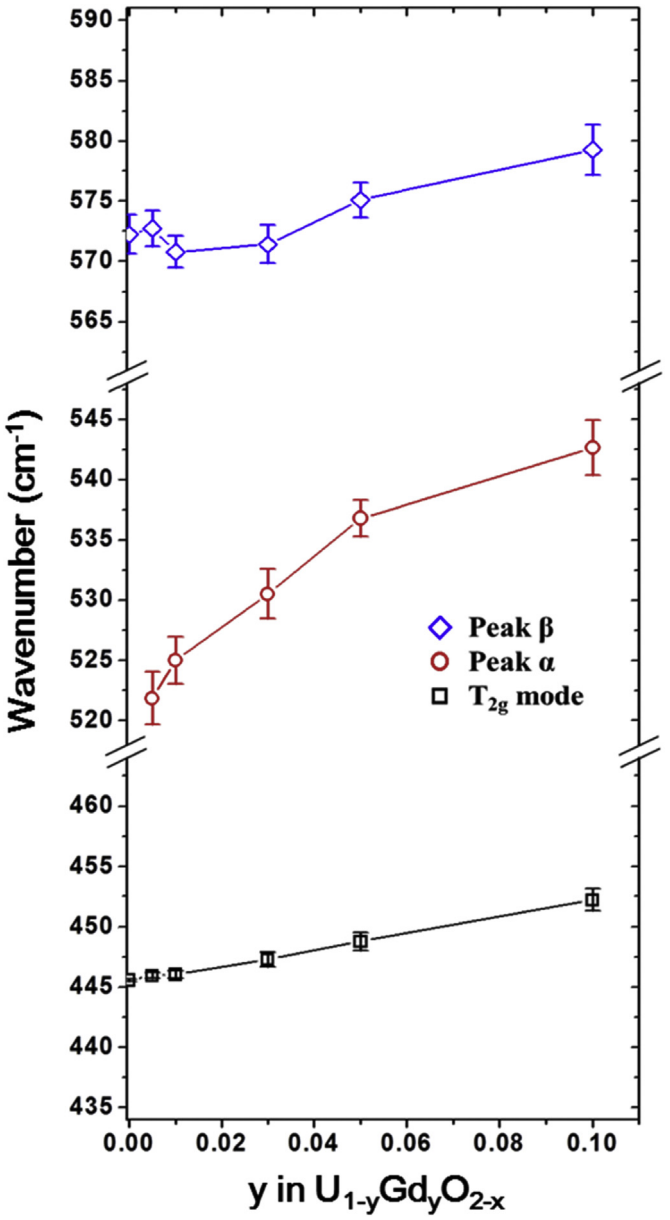

Fig. 5. The wavenumber with standard deviation of Lorentzian peak T_{2g}, α and β used to fit Raman spectra of $U_{1-y}Gd_yO_{2-x}$ solid solutions with Gd contents, y = 0.005, 0.01, 0.03, 0.05 and 0.1.

assignments are consistent with those of Desgranges et al. [26] who also interpreted a peak at this wavenumber in spectra measured on $(U,Nd)O_{2-x}$ as due to a local phonon mode associated with an oxygen-vacancy-induced lattice distortion. A similar peak was observed for $Ce_{1-y}RE_yO_{2-x}$ samples [36,37] and simulated using a Green's function model calculation [36]. These observations are consistent with the theoretical calculations of Park and Olander [38] for Gd-doped $UO_{2\pm x}$ which also indicated the presence of oxygen vacancies. Additionally, no peak α was observed in Raman spectra recorded on $U_{1-y}Th_yO_2$ samples [24], because Th^{4+} present in solid solution in $U^{4+}{}_{1-y}Th^{4+}{}_yO^{2-}{}_2$ does not require the creation of a significant number of oxygen vacancies to compensate for a charge imbalance. This strongly supports that peak α is an indication of the presence of oxygen vacancies. In this study, the areas of the T_{2g}, α, β and γ peaks (denoted as A_{T2g}, A_α, A_β and A_γ, respectively) were calculated and the area ratios relative to that of the T_{2g} peak area (A_α/A_{T2g}, A_β/A_{T2g} and A_γ/A_{T2g}) are plotted as a function of Gd content in Fig. 6. The A_α/A_{T2g} ratio which symbolizes the relative importance of oxygen vacancies in the fluorite lattice structure of UO_2 increases with increasing Gd content. As shown in Fig. 7 this increase is directly related to the increased oxygen deficiency determined using the lattice parameters obtained by XRD to calculate the value of x, Fig. 2. A similar peak shift was observed for the relative intensity of the 540 cm^{-1} band to T_{2g} band with a y value of $U_{1-y}La_yO_{2-y/2}$ [27]. The marked positive shift of peak α

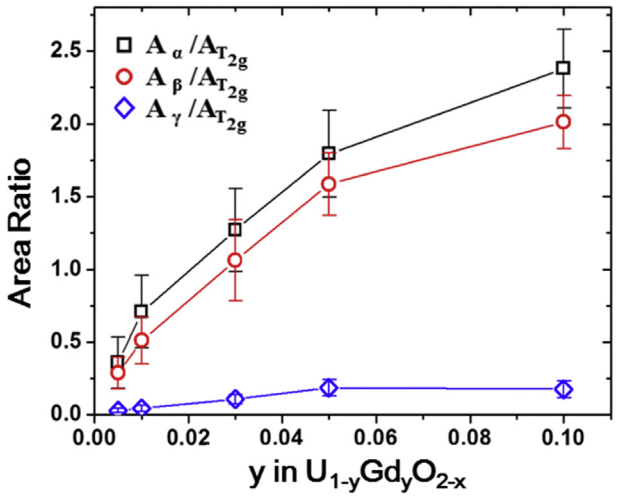

Fig. 6. Area ratio between peak α and T_{2g} (black square, A_α/A_{T2g}), peak β and T_{2g} (red circle, A_β/A_{T2g}) and peak γ and T_{2g} (blue diamond, A_γ/A_{T2g}) with y value of $U_{1-y}Gd_yO_{2-x}$ solid solutions. (For interpretation of the references to colour in this figure legend, the reader is referred to the web version of this article.)

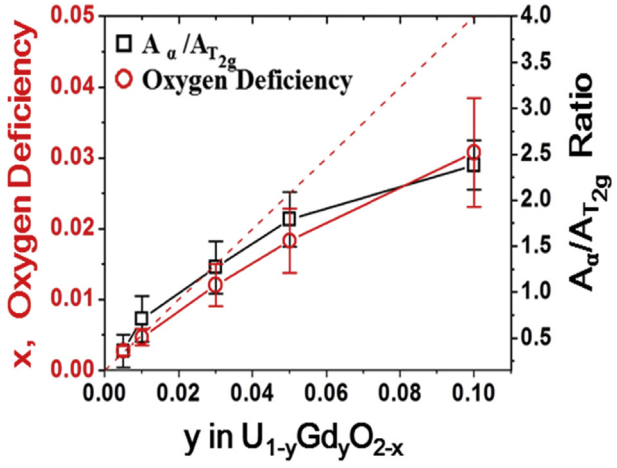

Fig. 7. Comparison of the A_α/A_{T2g} ratio with the calculated oxygen deficiency (x) of $U_{1-y}Gd_yO_{2-x}$ solid solutions with various Gd contents. Red dashed line represents the oxygen deficiency (x = y/2) of perfect $U_{1-y}Gd_yO_{2-y/2}$ solid solutions. (For interpretation of the references to colour in this figure legend, the reader is referred to the web version of this article.)

with increasing Gd content in Fig. 5 is to be expected as a result of the large lattice distortions caused by the large increase in oxygen vacancy concentration or dopant-vacancy clusters, as has been proposed in the mixed oxide defect model [38].

The peak β at ~575 cm^{-1} has been ascribed to a first order L-O phonon which arises due to crystal lattice disorder [34], although a peak at ~600 cm^{-1}, observed in a $Ce_{1-y}RE_yO_{2-x}$ sample [37] has been assigned to the formation of the MO_8-type complexes not involving oxygen vacancies [37,39,40]. A similar peak observed at ~575 cm^{-1} for UO_2 samples implanted with Kr and He^{2+} [32,41,42], and for hyperstoichiometric UO_{2+x} [23] has been assigned to lattice damage and the disorder induced by the presence of defects, respectively. Thus the increase in the A_β/A_{T2g} ratio with increasing Gd content represents a break down in selection rules due to the existence of oxygen vacancies. This break down of selection rules allows the forbidden first order L-O Raman scattering mode to be observed [43]. The disappearance of the bands in the region from 500 to 600 cm^{-1} in Raman spectra recorded on stoichiometric $U_{1-y}Nd_yO_2$ samples [26] and on $U_{1-y}La_yO_{2-y/2}$ samples during oxidation [27] strongly supports the association of peaks α and β with lattice defects due to oxygen vacancies. The positive shift of peak β with increasing Gd contents shows a similar tendency to that of peak T_{2g}.

The peak γ at ~630 cm^{-1} shown slightly in broad bands of all $U_{1-y}Gd_yO_{2-x}$ solid solutions has been ascribed to cuboctahedral clusters in the U_4O_9 phase [44]. This assignment was confirmed by Talip et al. during oxidation of $U_{1-y}La_yO_{2-y/2}$ [27]. Its general absence confirms the absence of this highly oxidized cluster in our specimens. The very slight increase in the A_γ/A_{T2g} ratio as the Gd content increases as shown in Fig. 6 may reflect oxidation during handling or a lack of reducing power during sintering. Such a surface oxidation may also result in the large difference between calculated oxygen deficiencies of $U_{1-y}Gd_yO_{2-x}$ solid solutions and those of fully reduced $U_{1-y}Gd_yO_{2-y/2}$ solid solutions (Fig. 2).

4. Conclusions

A series of $U_{1-y}Gd_yO_{2-x}$ specimens, with y = 0.005, 0.01, 0.03, 0.05 and 0.1, have been analyzed by XRD and Raman spectroscopy techniques.

XRD showed that an increase in Gd content caused a contraction in the fluorite lattice, indicated by the unit cell parameter, and a decrease in the O/M ratio indicating an increase in the oxygen deficiency of the lattice.

The Raman spectra showed an increased distortion of the fluorite lattice as the doping level increased. The shifts in Raman peak positions were consistent with a lattice contraction and with an increasingly defective structure.

An increase in the relative intensity for the Raman peak at 535 cm^{-1}, attributed to the presence of Gd dopant-oxygen vacancy clusters, compared to that of the peak at 445 cm^{-1}, attributed to the U-O symmetric stretching mode (T_{2g}) of the undisturbed fluorite lattice, confirmed the number of oxygen vacancies increased as the Gd doping level increased.

The position of the T_{2g} peak was found to vary linearly with Gd content indicating this shift could be used to determine the Gd content.

The characterization of $(U,Gd)O_{2-x}$ structures provides fundamental data to improve our understanding of spent nuclear fuel and has important implication for the characterization of nuclear fuel materials.

Acknowledgement

This work was supported by the National Research Foundation of Korea grant funded by the Korea government (Ministry of Science, ICT and Future Planning, MSIP).

References

[1] H. Kleykamp, The chemical state of the fission products in oxide fuels, J. Nucl. Mater 131 (1985) 221–246.
[2] R.J.M. Konings, T. Wiss, O. Beneš, Predicting material release during a nuclear reactor accident, Nat. Mater 14 (2015) 247–252.
[3] R.C. Ewing, Long-term storage of spent nuclear fuel, Nat. Mater 14 (2015) 252–257.
[4] J. Bruno, R.C. Ewing, Spent nuclear fuel, Elements 2 (2006) 343–349.
[5] J. Spino, P. Peerani, Oxygen stoichiometry shift of irradiated LWR-fuels at high burn-ups: review of data and alternative interpretation of recently published results, J. Nucl. Mater 375 (2008) 8–25.
[6] T.L. Markin, R.S. Street, E.C. Crouch, The uranium-cerium-oxygen ternary phase diagram, J. Inorg. Nucl. Chem. 32 (1970) 59–75.
[7] D. Shin, T.M. Besmann, Thermodynamic modeling of the $(U,La)O_{2\pm x}$ solid solution phase, J. Nucl. Mater 433 (2013) 227–232.
[8] J.W. McMurray, D. Shin, B.W. Slone, T.M. Besmann, Thermodynamic reassessment of U–Gd–O system, J. Nucl. Mater 452 (2014) 397–406.
[9] R.G. Brese, J.W. McMurray, D. Shin, T.M. Besmann, Thermodynamic

assessment of the U–Y–O system, J. Nucl. Mater 460 (2015) 5–12.
[10] T.K. Campbell, E.R. Gilbert, G.D. White, G.F. Piepel, B.J. Wrona, Oxidation behavior of nonirradiated UO_2, Nucl. Technol. 85 (1989) 160–171.
[11] L.E. Thomas, R.E. Einziger, H.C. Buchanan, Effect of fission products on air-oxidation of LWR spent fuel, J. Nucl. Mater 201 (1993) 310–319.
[12] G.-S. You, K.-S. Kim, D.-K. Min, S.-G. Ro, Oxidation kinetic changes of UO_2 by additive addition and irradiation, J. Nucl. Mater 277 (2000) 325–332.
[13] IAEA, reportInternational Atomic Energy Agency Report, IAEA-TECDOC-844.
[14] T. Wada, K. Noro, K. Tsukui, Behaviour of UO_2-Gd_2O_3 Fuel, International Confernce on Nuclear Fuel Performance, British Nuclear Energy Society in London, 1973.
[15] T. Ohmichi, S. Fukushima, A. Maeda, H. Watanabe, On the relation between lattice parameter and O/M ratio for Uranium dioxide-trivalent rare Earth oxide solid solution, J. Nucl. Mater 102 (1981) 40–46.
[16] H.G. Riella, M. Durazzo, M. Hirata, R.A. Nogueira, UO_2-Gd_2O_3 solid solution formation from wet and dry processes, J. Nucl. Mater 178 (1991) 204–211.
[17] J.-G. Kim, Y.-K. Ha, S.-D. Park, K.-Y. Jee, W.-H. Kim, Effect of a trivalent dopant, Gd^{3+}, on the oxidation of uranium dioxide, J. Nucl. Mater 297 (2001) 327–331.
[18] A.G. Leyva, D. Vega, V. Trimarco, D. Marchi, Homogeneity characterisation of sintered $(U,Gd)O_2$ pellets by X-ray diffraction, J. Nucl. Mater 303 (2002) 29–33.
[19] R.V. Krishnan, G. Panneerselvam, P. Manikandan, M.P. Antony, K. Nagarajan, Heat capacity and thermal expansion of Uranium-gadolinium mixed oxides, J. Nucl. Radiochem. Sci. 10 (2009) 19–26.
[20] M. Durazzo, F.B.V. Oliveira, E.F. Urano de Carvalho, H.G. Riella, Phase studies in the UO_2-Gd_2O_3 system, J. Nucl. Mater 400 (2010) 183–188.
[21] M. Schmitt, J. Popp, Raman spectroscopy at the beginning of the twenty-first century, J. Raman Spectrosc. 37 (2006) 20–28.
[22] D. Manara, B. Renker, Raman spectra of stoichiometric and hyper-stoichiometric uranium dioxide, J. Nucl. Mater 321 (2003) 233–237.
[23] H. He, D. Shoesmith, Raman spectroscopic studies of defect structures and phase transition in hyper-stoichiometric $UO_{(2+x)}$, Phys. Chem. Chem. Phys. 12 (2010) 8108–8117.
[24] R. Rao, R.K. Bhagat, N.P. Salke, A. Kumar, Raman spectroscopic investigation of thorium dioxide-Uranium dioxide (ThO_2-UO_2) fuel materials, Appl. Spectrosc. 68 (2014) 44–48.
[25] M. Razdan, D.W. Shoesmith, Influence of trivalent-dopants on the structural and electrochemical properties of Uranium dioxide (UO_2), J. Electrochem. Soc. 161 (2013) H105–H113.
[26] L. Desgranges, Y. Pontillon, P. Matheron, M. Marcet, P. Simon, G. Guimbretie, et al., Miscibility gap in the U–Nd–O phase Diagram: a new approach of nuclear oxides in the environment? Inorg. Chem. 51 (2012) 9147–9149.
[27] Z. Talip, T. Wiss, P.E. Raison, J. Paillier, D. Manara, J. Somers, et al., Raman and X-ray studies of Uranium-lanthanum-mixed oxides before and after air oxidation, J. Am. Ceram. Soc. 98 (2015) 2278–2285.
[28] F. Lebreton, D. Horlait, R. Caraballo, P.M. Martin, A.C. Scheinost, A. Rossberg, et al., Peculiar behavior of $(U,Am)O_{2-\delta}$ compounds for high americium contents evidenced by XRD, XAS, and Raman spectroscopy, Inorg. Chem. 54 (2015) 9749–9760.
[29] C. Jégou, R. Caraballo, J. De Bonfils, V. Broudic, S. Peuget, T. Vercouter, et al., Oxidizing dissolution of spent MOX47 fuel subjected to water radiolysis: solution chemistry and surface characterization by Raman spectroscopy, J. Nucl. Mater 399 (2010) 68–80.
[30] K. Iwasaki, T. Matsui, K. Yanai, R. Yuda, Y. Arita, T. Nagasaki, et al., Effect of Gd_2O_3 dispersion on the thermal conductivity of UO_2, J. Nucl. Sci. Technol. 46 (2009) 673–676.
[31] G.C. Allen, I.S. Butler, Characterisation of uranium oxides by micro-Raman spectroscopy, J. Nucl. Mater 144 (1987) 17–19.
[32] P.R. Graves, Raman microprobe spectroscopy of Uranium dioxide single crystals and ion implanted polycrystals, Appl. Spectrosc. 44 (1990) 1665–1667.
[33] G.M. Begun, R.G. Haire, W.R. Wilmarth, J.R. Peterson, Raman spectra of some actinide dioxides and of EuF_2, J. Less Common Met. 162 (1990) 129–133.
[34] T. Livneh, E. Sterer, Effect of pressure on the resonant multiphonon Raman scattering in UO_2, Phys. Rev. B 73 (2006) 085118.
[35] J. Schoenes, Electronic transitions, crystal field effects and phonons in UO_2, Phys. Rep. 63 (1980) 301–336.
[36] J.R. McBride, K.C. Hass, B.D. Poindexter, W.H. Weber, Raman and X-ray studies of $Ce_{1-x}RE_xO_{2-y}$, where RE=La, Pr, Nd, Eu, Gd, and Tb, J. Appl. Phys. 76 (1994) 2435–2441.
[37] L. Li, F. Chen, J.Q. Lu, M.F. Luo, Study of defect sites in $Ce_{1-x}M_xO_{2-\delta}$ ($x = 0.2$) solid solutions using Raman spectroscopy, J. Phys. Chem. A 115 (2011) 7972–7977.
[38] K. Park, D.R. Olander, Defect models for the oxygen potentials of gadolinium- and europium-doped urania, J. Nucl. Mater 187 (1992) 89–96.
[39] A. Nakajima, A. Yoshihara, M. Ishigame, Defect-induced Raman spectra in doped CeO_2, Phys. Rev. B 50 (1994) 13297–13307.
[40] T. Taniguchi, T. Watanabe, N. Sugiyama, A.K. Subramani, H. Wagata, N. Matsushita, et al., Identifying defects in ceria-based nanocrystals by UV resonance Raman spectroscopy, J. Phys. Chem. C 113 (2009) 19789–19793.
[41] G. Guimbretiere, L. Desgranges, A. Canizares, G. Carlot, R. Caraballo, C. Jegou, et al., Determination of in-depth damaged profile by Raman line scan in a pre-cut He^{2+} irradiated UO_2, Appl. Phys. Lett. 100 (2012) 251914.
[42] L. Desgranges, G. Guimbretière, P. Simon, F. Duval, A. Canizares, R. Omnee, et al., Annealing of the defects observed by Raman spectroscopy in UO_2 irradiated by 25MeV He^{2+} ions, Nucl. Instrum. Meth. Phys. Res. Sect. B Beam Interact. Mat. Atoms 327 (2014) 74–77.
[43] S.D. Senanayake, G.I.N. Waterhouse, A.S.Y. Chan, T.E. Madey, D.R. Mullins, H. Idriss, The reactions of water vapour on the surfaces of stoichiometric and reduced uranium dioxide: a high resolution XPS study, Catal. Today 120 (2007) 151–157.
[44] L. Desgranges, G. Baldinozzi, P. Simon, G. Guimbretière, A. Canizares, Raman spectrum of U_4O_9: a new interpretation of damage lines in UO_2, J. Raman Spectrosc. 43 (2012) 455–458.